



# Iron Oxide Nanoparticles Synthesized from Iron Waste as an Additive to Lubricants for Reducing Friction

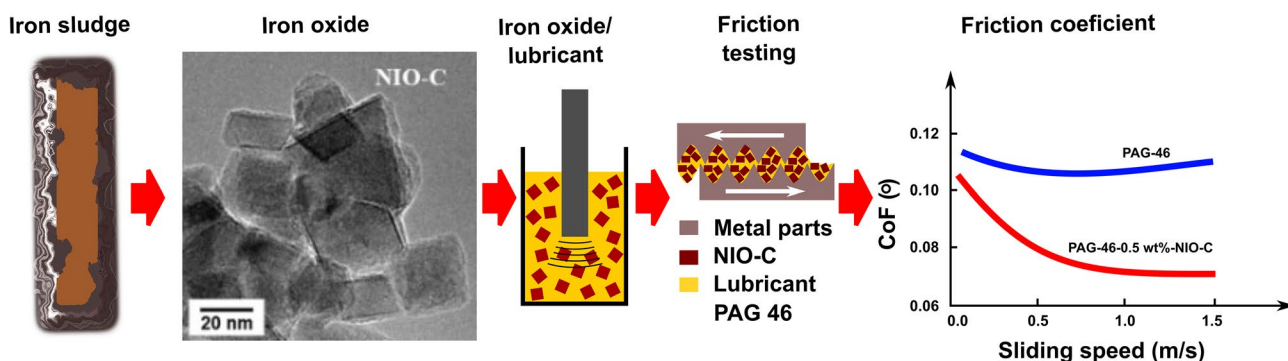
Suzana Gotovac Atlagić<sup>1</sup> · Sunčica Sukur<sup>1</sup> · Sanja Pržulj<sup>1</sup> · Yoshiyuki Hattori<sup>2</sup> · Khodor I. Nasser<sup>1,3</sup> · Mario Pisaturo<sup>4</sup> · Adolfo Senatore<sup>4</sup> · Radovan Kukobat<sup>5</sup> · Dragana Stević<sup>1</sup>

Received: 19 December 2022 / Accepted: 7 May 2023 / Published online: 24 May 2023  
© The Author(s), under exclusive licence to Springer Nature B.V. 2023

## Abstract

Development of sustainable routes for nanoparticle synthesis is one of the important research issues in waste management. Herein, we synthesized the nano iron oxide-cubic (NIO-C) nanoparticles from iron waste sludge for application as additive in polyethylene glycol (PAG46) lubricant. X-ray diffraction (XRD) evidenced the presence of maghemite as a dominant phase of the NIO-C nanoparticles, having (311) crystallographic plane at the diffraction angle of 35.27°. High-resolution transmission electron microscopy (HR-TEM) confirmed the presence of cubic maghemite of ~20 nm in size. The NIO-C nanoparticles served as the additive in the PAG46 lubricant, showing a decrease in the coefficient of friction by 46% at 25 °C and by 36% at 80 °C. Reducing the coefficient of friction was assigned to the cubic NIO-C fractions, enhancing the smoothness of the metal plates. This study describes economic and environmentally sustainable method for producing cubic maghemite nanoparticles.

## Graphical Abstract



**Keywords** Iron oxide · Nanoparticles · Tribology · Byproduct · Iron waste

## Statement of Novelty

Red mud waste from iron mines is one of the environmental problems nowadays. Utilization of the red mud waste for the synthesis of functional nanomaterials would reduce waste problems and give useful products. We report the synthesis of uniform iron oxide (maghemite type) nanoparticles from the red mud. Iron oxide nanoparticles are uniform in size,

serving as an additive to the lubricating oil. The iron oxide nanoparticles adsorb onto the surface between moving metal parts, decreasing the friction coefficient significantly. Hence, here we synthesized the iron oxide nanoparticles from the iron red mud waste and applied as an additive in the lubricants. This method is promising for the future large-scale synthesis of uniform iron oxide nanoparticles, contributing to waste reduction.

Extended author information available on the last page of the article

## Introduction

Nanoparticles can be synthesised by physical, chemical, and biological methods [1]. Nanoparticle synthesis requires salt precursors, and thereby supplying enough inorganic salts is a challenge for economical and environmentally friendly synthesis [2]. Metal oxide nanoparticles including  $\text{TiO}_2$ ,  $\text{SnO}_2$ ,  $\text{Al}_2\text{O}_3$ ,  $\text{ZnO}$ ,  $\text{ZrO}_2$ ,  $\text{Fe}_3\text{O}_4$  were synthesized from its salt precursors and used as additives for lubricants. Metal oxide nanoparticles dispersed in lubricants form protective films between rough metal surfaces, reducing the coefficient of friction by 5.36–65.4% [3, 4]. For example, addition of the  $\text{TiO}_2$  nanoparticles to lubricants is promising for reducing the coefficient of friction due to the protective film formation on the worn surfaces [5]. The  $\text{TiO}_2$  nanoparticles in lubricants enhanced load bearing capacity by 35% [6]. Lubricant containing 5 wt% of the  $\text{TiO}_2$  nanoparticles of ~50 nm in diameter resulted in reduction of the coefficient of friction by 15.2% and the coefficient of wear by 11.0% [7, 8]. Moreover,  $\text{Al}_2\text{O}_3$  nanoparticles of ~20 nm in diameter dispersed in lubricant were effective in reducing the coefficient of friction by 49.1% [9, 10]. In addition, iron oxide nanoparticles are efficient for reducing friction and wear, and have been widely studied due to low toxicity [11, 12, 13, 14, 15, 16, 17]. Thus, variety of metal oxides have shown high potential in reducing friction and wear.

Friction and wear occur at the interfaces between moving metals in mechanical systems [18]. Reducing friction and wear is necessary for efficient and effective function of mechanical systems such as vehicles and machines [19]. Furthermore, improving lubrication properties would significantly decrease the world's energy consumption [20]. Friction and wear consume ~23% of the world's energy, while ~20% of energy is used for friction. For example, at the internal energy combustion of a passenger car, only 21% of energy is used to move a car, while the rest of 79% accounts for energy losses including friction [21, 22]. Rough metal surfaces contribute to an increase in friction and wear, and thereby finding effective lubricants is a technical challenge for science and engineering [23]. Lubrication significantly reduces the coefficient of friction because the sliding metal surfaces are separated by layers of lubricant [24]. Nanoparticles dispersed into lubricants decrease the friction and wear coefficients, forming protective film (tribo-film) on sliding metal surfaces [25, 26, 27, 28]. Lubricants containing nanomaterials with low elastic modulus and high hardness are crucial for excellent lubricating properties [29, 30, 31]. Nanoparticles fill the rough surfaces, improving the smoothness of the sliding metal parts, leading to a significant decrease in the friction and wear coefficients [29].

The present study reports synthesis of iron oxide (maghemite) from an industrial byproduct of iron waste

sludge, contributing to waste reduction. Maghemite nanoparticles are biocompatible, being a favorable candidate for lubricant applications [32]. Maghemite nanoparticles were synthesized from iron waste sludge in the presence of cetrimonium bromide (CTAB), denoted as a nano iron oxide-cubic (NIO-C) structure. The NIO-C nanoparticles were used as an effective additive in PAG46 lubricant, reducing the coefficient of friction by 46% at 25 °C and by 36% at 80 °C. The presence of maghemite was confirmed with an X-ray diffraction (XRD), while the size and the interlayer distance was directly observed with a high-resolution transmission electron microscopy (HR-TEM). Effective tribological properties of maghemite dispersed in base oil were confirmed by measurements of the coefficient of friction against sliding speed.

## Experimental Procedure

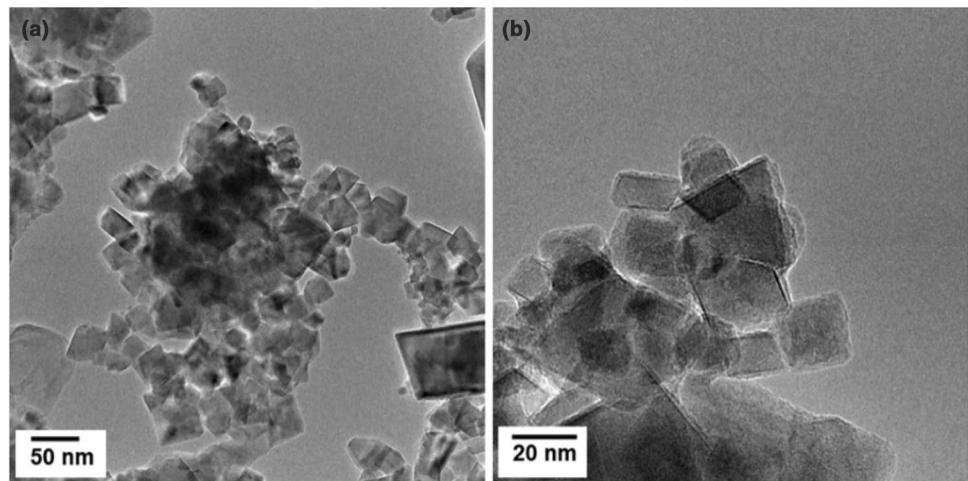
### Synthesis of the NIO-C Nanoparticles

The NIO-C nanoparticles were synthesized from the concentrated iron ionic solutions obtained from the waste sludge, located at an active iron mine near the city of Prijedor in Bosnia and Herzegovina. The synthesis procedure was adopted from our previous study described in the preceding literature [33, 34]. Extraction and purification of the sludge were conducted by open digesting the dry sludge with acids at the mass ratio of 10:1:1 = dry sludge: $\text{HNO}_3$  (65%): $\text{H}_2\text{SO}_4$  (98%) for 2 h. After digestion, the oxidized powder was dispersed in distilled water at the ratio of 1:100 = oxidized sludge:distilled water using ultrasonication at 60 Hz for 20 min. The dispersion was filtrated through the glass fiber filter (mesh 0.45  $\mu\text{m}$ ). Iron ions were separated by classical cationic separation with  $\text{NH}_4\text{Cl}$  and  $\text{NH}_4\text{OH}$ , followed by dissolution with conc.  $\text{HNO}_3$ . Atomic Absorption Spectrometer (Analyst 400, Perkin Elmer) served to measure concentrations of metal ions. Cationic surfactant cetrimonium bromide (CTAB) of molecular formula  $\text{C}_{19}\text{H}_{42}\text{BrN}$  served for micelle formation. The NIO-C nanoparticles were formed by precipitation in the basic medium ( $\text{NaOH}$ ) of  $\text{pH} = 13$ . The precipitate was dried at 105 °C for 2 h and treated at 600 °C for 2 h, as shown in SEM micrographs (Figure S1). The NIO-C nanoparticles were centrifuged (Technica Centric 200R) for 15 min at 5000 rpm, separated from the supernatant and dried at 105 °C in the air atmosphere. The NIO-C nanoparticles were further characterized.

### Characterization of Nanoparticles

An X-ray diffraction machine (XRD, Rigaku MiniFlex 300) with an X-ray source of  $\text{Cu-K}\alpha$ ,  $\lambda = 0.15418$  nm served for crystal structure characterization. A high-Resolution

**Fig. 1** HR-TEM micrographs representing the shape of the NIO-C nanoparticles observed at (a) low magnification and (b) high magnification



Transmission Electron Microscope (HRTEM, JEOL JEM 2010, 200 kV) and a scanning electron microscope (SEM, Hitachi S-500 20 kV) served for visual observations of the NIO-C nanoparticles. The NIO-C nanoparticle aggregates were ground with a mortar and pestle prior to the HR-TEM and SEM observations. The NIO-C nanoparticles were dispersed in ethanol and dropped onto the copper grid for HRTEM observations. Powder of the NIO-C nanoparticles was placed onto the conducting carbon tape for the SEM observations. An optical microscope (Sensofar Plu Neox3D) served for observation of the steel ball after the friction test.

### Tribology Tests

Tribology tests were conducted using rotational ball-on-disc tribometer (WAZAU TRM100) (Figure S2a). Efficiency of the NIO-C nanoparticles as an additive in polyethylene glycol (PAG46) lubricant was investigated as the coefficient of friction against the sliding speed of a ball over the steel disc. The PAG46 containing 0.5 wt% of the NIO-C nanoparticles was placed between an upper steel disc and a lower steel ball. The NIO-C nanoparticles were dispersed in PAG46 (Figure S2c) with a disperser tub (IKA T25 digital Ultra-Turrax) at 13 000 rpm for 30 min.

An upper steel disc (X155CrVMo12-1) (Figure S2b) had hardness of 60 HRC, the roughness average of 0.5  $\mu\text{m}$ , and diameter of 105 mm. A lower steel ball (X39Cr13) (Figure S2b) had hardness of  $57 \pm 3$  HRC, grade of 100, and diameter of 8 mm. The steel ball was completely immersed in a temperature-controlled lubricant bath of 350  $\text{cm}^3$ . The contact pressure of 1.50 GPa (normal load of 70 N) was applied at the ball/disc interface. Speed-sweep tests for Stribeck graphs were conducted by increasing/decreasing the speed from 0 to 2.0  $\text{m s}^{-1}$  in 4 min at the constant pressure. We repeated the speed pattern for 6 times. The tests were performed at the temperatures of 25  $^\circ\text{C}$  and 80  $^\circ\text{C}$ .

## Results and Discussion

### Shape of the NIO Nanoparticles

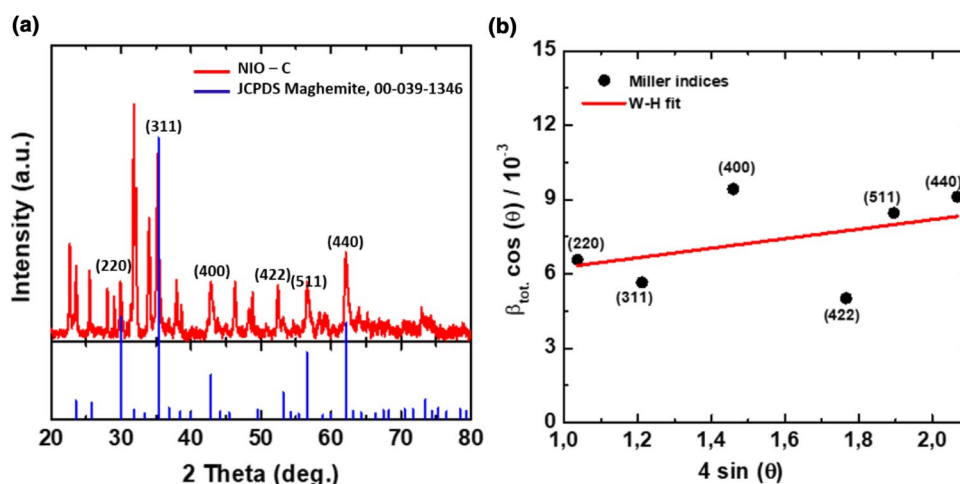
The shape of the nano iron oxide (NIO) nanoparticles was investigated using HR-TEM microscopy. The NIO nanoparticles consist of agglomerates of small cubic crystals that are uniform in size, denoted as the nano iron oxide-cubic (NIO-C) nanoparticles (Fig. 1a, Figure S3). Agglomerates of the NIO-C nanoparticles have the size of several hundreds of nanometers. Aggregation of the NIO-C nanoparticles can be assigned to the presence of van der Waals attractive forces, giving well-contacted cubic nanoparticles (Fig. 1b) [35]. SEM micrographs show the presence of large aggregates of the NIO-C nanoparticles (Figure S1a, b). We estimated the external surface area of the NIO-C nanoparticles assuming the cubic shape of the NIO-C nanoparticles. The external surface area ( $S_{\text{ex}}$ ) of the NIO-C nanoparticles was calculated as follows:

$$S_{\text{ex}} = \frac{\bar{A}}{\rho \cdot \bar{V}} \cdot 10^3 (\text{m}^2 \text{g}^{-1}) \quad (1)$$

where  $\bar{A}$  is the average area of the NIO-C nanoparticle determined as the edge length square ( $\bar{a}^2$ ,  $\text{nm}^2$ ),  $\rho$  is the density of the NIO-C nanoparticles (4.90  $\text{g cm}^{-3}$ ) referred to maghemite, and  $\bar{V}$  is the average volume of the NIO-C nanoparticles, determined as the edge length cube ( $\bar{a}^3$ ,  $\text{nm}^3$ ) [36]. The NIO-C nanoparticles have the external surface area of 12  $\text{m}^2 \text{g}^{-1}$ , according to our estimation. The NIO-C nanoparticles have a small internal porosity according to nitrogen adsorption analysis [37]. Thus, the external surface area of the NIO-C nanoparticles should be nearly equal to the total surface area of 12  $\text{m}^2 \text{g}^{-1}$ .

The NIO-C nanoparticles were formed at the controlled conditions of synthesis such as total Fe concentration, temperature, and pH [38]. Oxidized Fe ions in the presence of

**Fig. 2** Crystallinity of the NIO-C nanoparticles by XRD. **a** XRD patterns of the NIO-C nanoparticles and JCPDS cards of maghemite. **b** W–H plot for crystal size and macrostrain determination



CTAB at the temperature of 105 °C led to the slow Fe ion diffusion, giving the NIO-C nanoparticles of relatively uniform shape. Shape and size of the NIO-C nanoparticles can be changed by changing the concentration of Fe ions, temperature, and pH.

### Crystallinity of NIO-C and Crystal Sizes Determined by Scherrer and Williamson-Hall Methods

The XRD pattern shows the crystal structure of the NIO-C nanoparticles (Fig. 2a). The peaks at diffraction angles of 30.03°, 35.27°, 42.80°, 52.37°, 56.56° and 62.25° correspond to the crystal planes of (220), (311), (400), (422), (511), and (440) [39, 40]. The crystal sizes were calculated using Scherrer and Williamson-Hall (W–H) equations for comparison. Scherrer's equation is used for determination of the crystal size of powders from the crystalline planes as follows: [41]

$$L = \frac{K\lambda}{\beta \cos(\theta)} \quad (2)$$

where  $K$  is the shape factor that is close to unity (0.90),  $\lambda$  is the wavelength of X-rays of 0.15406 nm for Cu  $K\alpha$  X-ray source,  $\beta$  is the line broadening at half maximum of the diffraction peak,  $\theta$  is the Bragg angle. W–H and Scherrer equations were used to determine the crystal sizes, considering the X-ray diffraction peaks of the NIO-C nanoparticles. W–H method considers the size broadening and the strain broadening as follows: [42]

$$\beta \cos(\theta) = \epsilon 4 \sin(\theta) + \frac{K\lambda}{D} \quad (3)$$

where  $\epsilon$  is the strain, and  $D$  is the crystal size. The crystal size and the strain were determined from the intercept and slope of  $\beta \cos(\theta)$  vs.  $4 \sin(\theta)$  (Fig. 2b).

**Table 1** Parameters of the XRD patterns with the peak positions, crystal size ( $L$ ) determined by Scherrer, and the crystal size ( $D$ ) and microstrain determined by W–H equation

2 theta (deg)	Miller indices	Scherrer L (nm)	W–H D (nm)	Macrostrain $\epsilon/10^{-3}$
30.03	(220)	23.71	75.24	4.34
35.27	(311)	24.50		
42.80	(400)	24.14		
52.37	(422)	31.18		
56.56	(511)	18.89		
62.25	(440)	20.94		

The crystal sizes of the NIO-C nanoparticles were estimated using Scherrer and W–H methods (Table 1). Scherrer method gives the crystal sizes at the diffraction planes. The crystal sizes at the crystallographic faces of (220), (311), (400), (422), (511), and (440) are in the range of 18–24 nm. W–H method is more rigorous than Scherrer method, giving the average NIO-C size of 75.24 nm, considering the aforementioned crystal faces. Thus, the large crystal size by W–H method applies to the entire crystal, while Scherrer method gives the crystal sizes at the particular crystallographic faces.

The HR-TEM micrograph shows the crystal lattice of the NIO-C nanoparticles, confirming high crystallinity (Fig. 3). The NIO-C nanoparticles have a well-ordered structure of maghemite without defects in the crystal lattice. The interlayer distance of the NIO-C nanoparticles ranges from 0.15 to 0.30 nm (Table 2), as estimated from XRD crystallographic planes. Fast Fourier Transform (FFT) of HR-TEM shows the interlayer distance of 0.25 nm (Fig. 3), corresponding to that of (311) crystallographic plane (Table 2). Interlayer distance from XRD crystallographic plane (311) coincides with that estimated from the FFT-HRTEM

**Fig. 3** HR-TEM of the NIO-C nanoparticles and its corresponding FFT micrograph, showing the interlayer distance between the crystalline planes

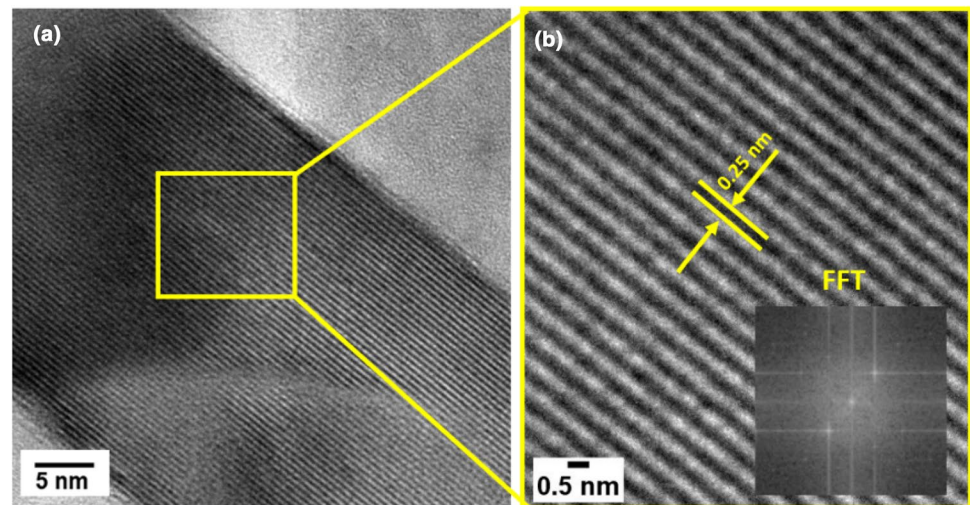


**Table 2** Interlayer distances at the crystalline planes estimated from Bragg diffraction law

2 theta (deg)	Miller indices	d (nm)
30.03	(220)	0.30
35.27	(311)	0.25
42.80	(400)	0.21
52.37	(422)	0.17
56.56	(511)	0.16
62.25	(440)	0.15

micrograph, confirming the presence of the maghemite nanoparticles [43].

The particle size distribution histogram was referred from the TEM images by measuring the size of the NIO-C nanoparticles (Fig. 4a). The NIO-C nanoparticles have narrow particle size distribution, ranging from 10 to 60 nm. The NIO-C nanoparticles of  $21.60 \pm 1.96$  nm in size are dominant. A comparison plot between crystal sizes determined by different methods shows that the NIO-C nanoparticle size by W–H method is as high as 75.24 nm, while the particle sizes determined by Scherrer method and HR-TEM observation show similar sizes of 23.89 nm on average and 21.60 nm, respectively (Fig. 4b). The crystal size of the NIO-C nanoparticles determined by W–H method is the highest because the crystallographic faces of the entire crystal were considered, while the crystal sizes by Scherrer method and TEM observation are similar because the edge length was measured at particular crystallographic planes.

### Effect of the NIO-C Nanoparticles on Friction

The NIO-C nanoparticles, owing to its nanoscale size, can fit onto rough metal surfaces, filling the grooves and reducing the friction between the metal parts in motion. Stribeck graphs (Fig. 5) show an effect of PAG46 lubricant on the

coefficient of friction at 25 and 80 °C, containing dispersed NIO-C nanoparticles between the sliding metal surfaces. The lubricant layer was located at the interface between the sliding metal surfaces. The coefficient of friction of the pure PAG46 lubricant against the sliding speed has almost constant tendency, suggesting that the pure lubricant does not significantly reduce the coefficient of friction (Fig. 5a). The lubricant containing 0.5 wt% of the NIO-C nanoparticles reduces the coefficient of friction by 46% at the temperature of 25 °C. Decrease in the coefficient of friction can be explained by a thin NIO-C layer formation on the metal surface. The layers of the NIO-C nanoparticles adsorb onto the rough metal surface, reducing the roughness and the coefficient of friction consequently. In contrast, the coefficient of friction was reduced by 36% at the temperature of 80 °C (Fig. 5b). Reducing the coefficient of friction at 80 °C was smaller than that at 25 °C due to the general tendency of a decrease in lubricant viscosity with temperature. Thus, when viscosity is low (at 80 °C), the NIO-C nanoparticles cannot entrap well onto the grooves on the metal surface, giving a higher coefficient of friction. Oppositely, when viscosity is high (at 25 °C), the NIO-C nanoparticles are firmly attached on the metal surface, smoothening the surface and giving a low coefficient of friction.

The lubrication mechanism in the presence and absence of the NIO-C nanoparticles as an additive can be illustrated schematically as shown in Fig. 6. Two steel discs lubricated with oil without the NIO-C nanoparticles (Fig. 6a) do not show a decrease in the coefficient of friction against sliding speed (corresponding to the blue line in Figs. 4a and b) because the surfaces come into contact. The grooves on the steel disc scratch each other and the coefficient of friction remains almost constant against the sliding speed. On the other hand, lubricant PAG46 containing dispersed NIO-C nanoparticles reduces the coefficient of friction against sliding speed (corresponding to the red line in Figs. 5a and b)

**Fig. 4** NIO-C crystal size. **a** Histogram of the size distribution. **b** Comparison plot of the sizes determined by W–H method, Scherrer method, and TEM observation. Crystal size by Scherrer method represents the average from all crystallographic planes

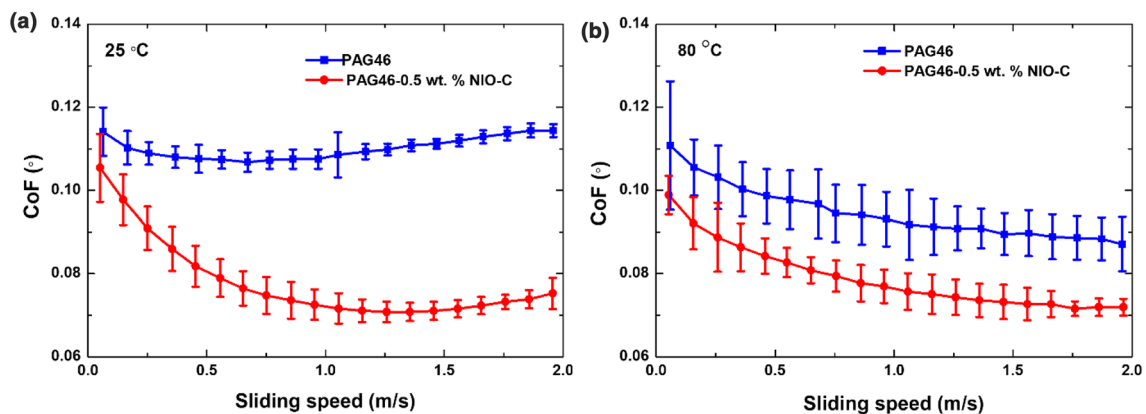
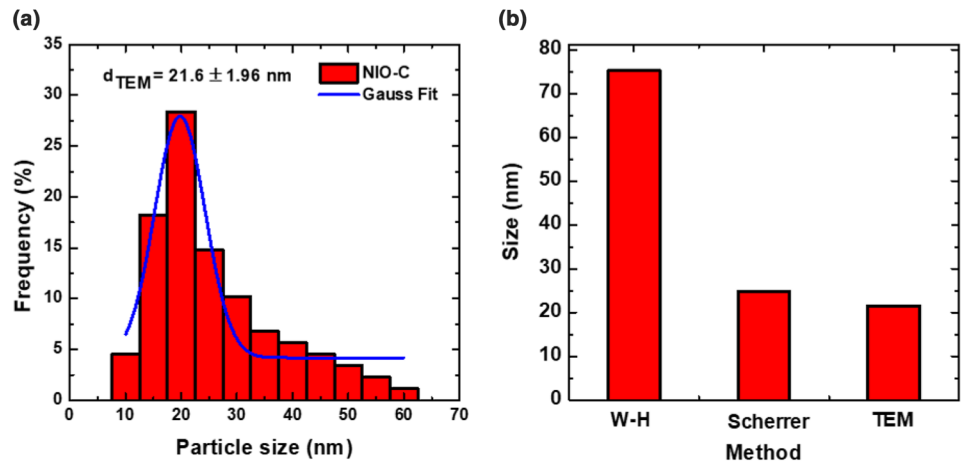
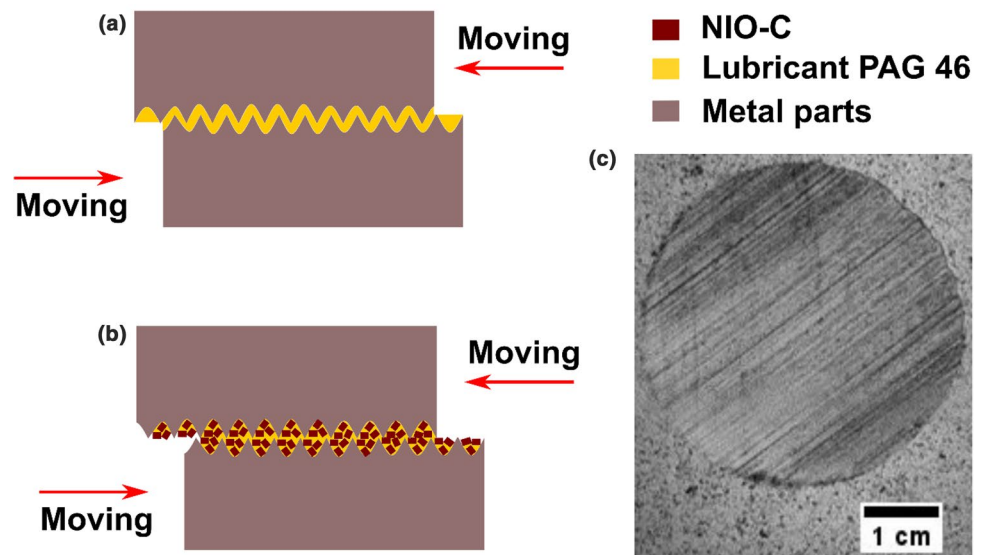


**Fig. 5** Stribeck curves for the NIO-C nanoparticles. **a** Lubricant temperature: 25 °C. **b** Lubricant temperature: 80 °C. The average contact pressure of 1.50 GPa and the sliding speed of the steel ball of  $1 \text{ m s}^{-1}$  were applied

**Fig. 6** Schematic representation of the rough metal surfaces in contact sliding in opposite directions: **a** Rough metal surfaces lubricated with PAG-46. **b** Rough metal surfaces lubricated with PAG46-NIO-C. **c** Optical micrograph of the steel ball after friction test



because the nanoparticles fill the grooves on the steel surface (Fig. 6c). Steel surfaces with the nanoparticles filling the

grooves become smooth, leading to a decrease in the coefficient of friction.

## Summary

The NIO-C nanoparticles of high crystallinity and uniform size distribution were synthesized from the Fe ionic solutions remediated from the waste sludge of the Fe mine. We demonstrated production of the NIO-C nanoparticles from Fe waste sludge and its potential application as an additive in base oil (PAG46). The NIO-C nanoparticles (0.5 wt%) dispersed in PAG46 decreased the coefficient of friction by 46% at 25 °C and by 36% at 80 °C. The NIO-C nanoparticles fill the grooves on the metal surfaces, smoothening the surface and decreasing the coefficient of friction. The NIO-C nanoparticles synthesized from the Fe waste sludge are promising for future application as additives in lubricants.

**Supplementary Information** The online version contains supplementary material available at <https://doi.org/10.1007/s12649-023-02165-w>.

**Acknowledgements** The authors thank the following founding sources: Ministry of Scientific-Research Development, Higher Education and Information Society of the Republic of Srpska, Bosnia and Herzegovina (Grant No. 19.032/961-151/19) and European Institute for Innovation and Technology (EIT RM) for grant number 16320.

**Author Contributions** Original idea for this work was proposed by SGA. Material preparation was performed by DS. Data collection and analysis were performed by YH, MP, AS and DS. The first draft of the manuscript was written by DS. Suggestions about the manuscript improvements were given by RK, SS, KIN and SP. All authors read and approved the final manuscript.

**Funding** This work was supported by Ministry of Scientific-Research Development, Higher Education and Information Society of the Republic of Srpska, Bosnia and Herzegovina (grant number 19.032/961–151/19) and European Institute for Innovation and Technology (EIT RM) for grant number 16320.

**Data Availability** Enquiries about data availability should be directed to the authors.

## Declarations

**Competing Interest** The authors declare that they have no known competing financial interests of personal relationships that could have appeared to influence the work reported in this paper.

## References


1. Ali, A., Zafar, H., Zia, M., Haq, I., Phull, A.R., Ali, J.S., Hussain, A.: Synthesis, characterization, applications, and challenges of iron oxide nanoparticles. *Nanotechnol. Sci. Appl.* **9**, 49–67 (2016). <https://doi.org/10.2147/NSA.S99986>
2. Sayed, F.N., Polshettiwar, V.: Facile and sustainable synthesis of shaped iron oxide nanoparticles: effect of iron precursor salts on the shapes of iron oxides. *Sci. Rep.* **5**(1), 9733 (2015). <https://doi.org/10.1038/srep09733>
3. Uflyand, I.E., Zhinzhiro, V.A., Burlakova, V.E.: Metal-containing nanomaterials as lubricant additives: state-of-the-art and future development. *Friction* **7**(2), 93–116 (2019). <https://doi.org/10.1007/s40544-019-0261-y>
4. Kong, L., Sun, J., Bao, Y.: Preparation, characterization and tribological mechanism of nanofluids. *RSC Adv.* **7**(21), 12599–12609 (2017). <https://doi.org/10.1039/C6RA28243A>
5. Ingole, S., Charanpahari, A., Kakade, A., Umare, S.S., Bhatt, D.V., Menghani, J.: Tribological behavior of nano TiO<sub>2</sub> as an additive in base oil. *Wear* **301**(1), 776–785 (2013). <https://doi.org/10.1016/j.wear.2013.01.037>
6. Shenoy, B.S., Binu, K.G., Pai, R., Rao, D.S., Pai, R.S.: Effect of nanoparticles additives on the performance of an externally adjustable fluid film bearing. *Tribol. Int.* **45**(1), 38–42 (2012). <https://doi.org/10.1016/j.triboint.2011.10.004>
7. Arumugam, S., Sriram, G.: Preliminary study of nano-and micro-scale TiO<sub>2</sub> additives on tribological behavior of chemically modified rapeseed oil. *Tribol. Trans.* **56**(5), 797–805 (2013)
8. Kao, M.-J., Lin, C.-R.: Evaluating the role of spherical titanium oxide nanoparticles in reducing friction between two pieces of cast iron. *J. Alloys Compd.* **483**(1), 456–459 (2009). <https://doi.org/10.1016/j.jallcom.2008.07.223>
9. N. Mohan, M. Sharma, R. Singh, and N. Kumar, “Tribological properties of automotive lubricant SAE 20W-40 containing nano-Al<sub>2</sub>O<sub>3</sub> particles,” SAE Technical Paper, 2014.
10. Krishnamurthy, A., Abdul Razak, K., Halemani, B.S., Buradi, A., Afzal, A., Ahamed Saleel, C.: Performance enhancement in tribological properties of lubricants by dispersing TiO<sub>2</sub> nanoparticles. *Mater. Today Proc.* **47**, 6180–6184 (2021). <https://doi.org/10.1016/j.matpr.2021.05.083>
11. Xiang, L., Gao, C., Wang, Y., Pan, Z., Hu, D.: Tribological and tribochemical properties of magnetite nanoflakes as additives in oil lubricants. *Particuology* **17**, 136–144 (2014). <https://doi.org/10.1016/j.partic.2013.09.004>
12. Iida, S., Hidaka, Y.: Influence of the iron oxide layer on lubricating properties in seamless pipe hot rolling. *Tetsu-Hagane* **94**(7), 244–250 (2008). <https://doi.org/10.2355/tetsuohagane.94.244>
13. De Oliveira, L.R., Rodrigues, T.A., Costa, H.L., da Silva Jr, W.M.: Scuffing resistance of polyalphaolefin (PAO)-based nanolubricants with oleic acid (OA) and iron oxide nanoparticles. *Mater. Today. Commun.* (2022). <https://doi.org/10.1016/j.mtcomm.2022.103837>
14. Ma, F., et al.: Evaluation of tribological performance of oxide nanoparticles in fully formulated engine oil and possible interacting mechanism at sliding contacts. *Surf. Interfaces* (2021). <https://doi.org/10.1016/j.surfin.2021.101127>
15. Lotfi, R., van Duin, A.C.T., Biswas, M.M.: Molecular dynamics simulations of perfluoropolyether lubricant degradation in the presence of oxygen, water, and oxide nanoparticles using a ReaxFF reactive force field. *J. Phys. Chem. C* **122**(5), 2684–2695 (2018). <https://doi.org/10.1021/acs.jpcc.7b09660>
16. Majeed, F.S.A., Yusof, N.B.M., Suhaimi, M.A., Elsit, N.M.: Effect of paraffin oil with XGnP and Fe<sub>2</sub>O<sub>3</sub> nanoparticles on tribological properties. *Mater. Today Proc.* **27**, 1685–1688 (2020). <https://doi.org/10.1016/j.matpr.2020.03.576>
17. Liñeira del Río, J.M., et al.: Tribological behavior of nanolubricants based on coated magnetic nanoparticles and trimethylolpropane trioleate base oil. *Nanomaterials* **10**(4), 683 (2020). <https://doi.org/10.3390/nano10040683>
18. Czichos, H.: Introduction to Friction and Wear. In: Composite Materials Series, pp. 1–23. Elsevier, Amsterdam (1986). <https://doi.org/10.1016/B978-0-444-42524-9.50005-3>
19. Yazawa, S., Minami, I., Prakash, B.: Reducing friction and wear of tribological systems through hybrid tribofilm consisting of coating and lubricants. *Lubricants* **2**(2), 90–112 (2014). <https://doi.org/10.3390/lubricants2020090>
20. Bronshteyn, L.A., Kreiner, J.H.: Energy efficiency of industrial oils. *Tribol. Trans.* **42**(4), 771–776 (1999). <https://doi.org/10.1080/10402009908982281>

21. Holmberg, K., Erdemir, A.: Influence of tribology on global energy consumption, costs and emissions. *Friction* **5**(3), 263–284 (2017). <https://doi.org/10.1007/s40544-017-0183-5>
22. Holmberg, K., Erdemir, A.: The impact of tribology on energy use and CO<sub>2</sub> emission globally and in combustion engine and electric cars. *Tribol. Int.* **135**, 389–396 (2019). <https://doi.org/10.1016/j.triboint.2019.03.024>
23. Bachchhav, B., Bagchi, H.: Effect of surface roughness on friction and lubrication regimes. *Mater. Today Proc.* **38**, 169–173 (2021). <https://doi.org/10.1016/j.matpr.2020.06.252>
24. Holmberg, K.: The mechanism of lubrication in low speed rolling contacts. *J. Tribol.* **111**(4), 703–707 (1989). <https://doi.org/10.1115/1.3261998>
25. Zhang, Y., et al.: Synthesis of reduced graphene oxide/Cu nanoparticle composites and their tribological properties. *RSC Adv.* **3**(48), 26086–26093 (2013). <https://doi.org/10.1039/C3RA42478B>
26. Li, X., Yang, W.: Simulating fullerene ball bearings of ultra-low friction. *Nanotechnology* **18**(11), 115718 (2007). <https://doi.org/10.1088/0957-4484/18/11/115718>
27. Jason, Y.J.J., How, H.G., Teoh, Y.H., Chuah, H.G.: A Study on the tribological performance of nanolubricants. *Processes* **8**(11), 1372 (2020). <https://doi.org/10.3390/pr8111372>
28. Tang, Z., Li, S.: A review of recent developments of friction modifiers for liquid lubricants (2007–present). *Curr. Opin. Solid State Mater. Sci.* **18**(3), 119–139 (2014). <https://doi.org/10.1016/j.cossms.2014.02.002>
29. Azman, N.F., Samion, S.: Dispersion stability and lubrication mechanism of nanolubricants: a review. *Int. J. Precis. Eng. Manuf.-Green Technol.* **6**(2), 393–414 (2019). <https://doi.org/10.1007/s40684-019-00080-x>
30. Yu, W., Xie, H.: A review on nanofluids: preparation, stability mechanisms, and applications. *J. Nanomater.* **2012**, 1–17 (2012). <https://doi.org/10.1155/2012/435873>
31. Lin, J., Wang, L., Chen, G.: Modification of graphene platelets and their tribological properties as a lubricant additive. *Tribol. Lett.* **41**(1), 209–215 (2011). <https://doi.org/10.1007/s11249-010-9702-5>
32. Gupta, A.K., Gupta, M.: Synthesis and surface engineering of iron oxide nanoparticles for biomedical applications. *Biomaterials* **26**(18), 3995–4021 (2005). <https://doi.org/10.1016/j.biomaterials.2004.10.012>
33. Suzana Gotovac Atlagić, Vladimiro dal Santo and Adolfo Senatore, “Synthesis of the Hematite Nanoparticle from the Iron Mine Waste Sluges Accumulations,” BAP203346A, Mar. 2021 [Online]. Available: [https://www.ipr.gov.ba/upload/documents/dokumenti\\_podstrance/glasnici/glasnik\\_br.3\\_2021.pdf](https://www.ipr.gov.ba/upload/documents/dokumenti_podstrance/glasnici/glasnik_br.3_2021.pdf)
34. Stević, D., et al.: Hematite core nanoparticles with carbon shell: potential for environmentally friendly production from iron mining sludge. *J. Mater. Eng. Perform.* **25**(8), 3121–3127 (2016). <https://doi.org/10.1007/s11665-016-1964-0>
35. Lalatonne, Y., Richardi, J., Pileni, M.P.: Van der waals versus dipolar forces controlling mesoscopic organizations of magnetic nanocrystals. *Nat. Mater.* **3**(2), 121–125 (2004). <https://doi.org/10.1038/nmat1054>
36. Lucas, I.T., Durand-Vidal, S., Dubois, E., Chevalet, J., Turq, P.: Surface charge density of maghemite nanoparticles: role of electrostatics in the proton exchange. *J. Phys. Chem. C* **111**(50), 18568–18576 (2007). <https://doi.org/10.1021/jp0743119>
37. Nadejde, C., et al.: Tannic acid- and natural organic matter-coated magnetite as green Fenton-like catalysts for the removal of water pollutants. *J. Nanoparticle Res.* **17**(12), 476 (2015). <https://doi.org/10.1007/s11051-015-3290-0>
38. Taylor, R.M., Schwertmann, U.: Maghemite in soils and its origin: II. Maghemite syntheses at ambient temperature and pH 7. *Clay Miner.* **10**(4), 299–310 (1974). <https://doi.org/10.1180/claymin.1974.010.4.08>
39. Busquets, M.A., Fernández-Pradas, J.M., Serra, P., Estelrich, J.: Superparamagnetic nanoparticles with efficient near-infrared photothermal effect at the second biological window. *Molecules* **25**(22), 5315 (2020). <https://doi.org/10.3390/molecules25225315>
40. Kim, W., et al.: A new method for the identification and quantification of magnetite–maghemite mixture using conventional X-ray diffraction technique. *Talanta* **94**, 348–352 (2012). <https://doi.org/10.1016/j.talanta.2012.03.001>
41. Patterson, A.L.: The scherrer formula for X-ray particle size determination. *Phys. Rev.* **56**(10), 978–982 (1939). <https://doi.org/10.1103/PhysRev.56.978>
42. Williamson, G.K., Hall, W.H.: X-ray line broadening from filed aluminium and wolfram. *Acta Metall.* **1**(1), 22–31 (1953). [https://doi.org/10.1016/0001-6160\(53\)90006-6](https://doi.org/10.1016/0001-6160(53)90006-6)
43. Singh, M., Ulbrich, P., Prokopec, V., Svoboda, P., Šantavá, E., Štěpánek, F.: Vapour phase approach for iron oxide nanoparticle synthesis from solid precursors. *J. Solid State Chem.* **200**, 150–156 (2013). <https://doi.org/10.1016/j.jssc.2013.01.037>

**Publisher's Note** Springer Nature remains neutral with regard to jurisdictional claims in published maps and institutional affiliations.

Springer Nature or its licensor (e.g. a society or other partner) holds exclusive rights to this article under a publishing agreement with the author(s) or other rightsholder(s); author self-archiving of the accepted manuscript version of this article is solely governed by the terms of such publishing agreement and applicable law.

## Authors and Affiliations

Suzana Gotovac Atlagić<sup>1</sup> · Sunčica Sukur<sup>1</sup> · Sanja Pržulj<sup>1</sup> · Yoshiyuki Hattori<sup>2</sup> · Khodor I. Nasser<sup>1,3</sup> · Mario Pisaturo<sup>4</sup> · Adolfo Senatore<sup>4</sup> · Radovan Kukobat<sup>5</sup> · Dragana Stević<sup>1</sup> 

✉ Dragana Stević  
dragana.stevic@pmf.unibl.org

<sup>1</sup> Department of Chemistry, Faculty of Natural Sciences and Mathematics, University of Banja Luka, Mladena Stojanovića 2, 78000 Banja Luka, Bosnia and Herzegovina

<sup>2</sup> Division of Chemistry and Materials, Faculty of Textile Science and Technology, Shinshu University, Ueda 386-8567, Japan

<sup>3</sup> Laboratory of Thermophysical and Tribological Properties, Nafomat Group, Department of Applied Physics, University of Santiago de Compostela, 15782 Santiago de Compostela, Spain

<sup>4</sup> Department of Industrial Engineering, University of Salerno, Via Giovanni Paolo II 132, 84084 Fisciano, Salerno, Italy

<sup>5</sup> Department of Chemical Engineering and Technology, Faculty of Technology, University of Banja Luka, V.S. Stepanovica 73, 78000 Banja Luka, Bosnia and Herzegovina